第 31 卷第 2 期
2015 年 2 月

无 机 化 学 学 报
CHINESE JOURNAL OF INORGANIC CHEMISTRY

Vol.31 No.2
385-398

Fe_2BiTaO_7 纳米催化剂的组织结构及光催化性能

栾景飞* 胡文华 陈标杭 裴冬华

(南京大学环境学院污染控制与资源化研究国家重点实验室,南京 210023)

摘要: 用固相反应合成法合成了光催化剂 Fe_2BiTaO_7,通过 XRD、SEM、TEM、紫外-可见漫反射等表征方法对其组织结构及光催化性能进行了研究。结果表明 Fe_2BiTaO_7 为立方晶系烧绿石结构,空间群为 *Fd*3*m*,禁带宽度为 1.72 eV。通过比较 Fe_2BiTaO_7、P25 TiO_2、掺氮 TiO_2 和 Bi_2InTaO_7 的可见光光催化降解罗丹明 B,发现 Fe_2BiTaO_7 降解效果及催化活性均高于其它催化剂,并且 Fe_2BiTaO_7 降解罗丹明 B 效率是掺氮二氧化钛的 1.5 倍。Fe_2BiTaO_7 降解罗丹明 B 的曲线符合一级动力学, 一级动力学常数为 0.022 93 min^{-1}。研究了罗丹明 B 可能的降解路径和 Fe_2BiTaO_7 在可见光下降解苯酚的效果。Fe_2BiTaO_7(可见光)光催化剂系统适用于纺织工业废水处理。

关键词: 催化作用; Fe_2BiTaO_7; 光学性能; 可见光; 光催化降解; 罗丹明 B

中图分类号: O643.36 **文献标识码**: A **文章编号**: 1001-4861(2015)02-0385-14

DOI: 10.11862/CJIC.2015.046

Structural and Photocatalytic Properties of Fe_2BiTaO_7 Nanocatalyst

LUAN Jing-Fei* HU Wen-Hua CHEN Biao-Hang PEI Dong-Hua

(*State Key Laboratory of Pollution Control and Resource Reuse, School of the Environment, Nanjing University, Nanjing* 210023, *China*)

Abstract: Fe_2BiTaO_7 powder photocatalyst was synthesized by a solid state reaction method. The structural and photocatalytic properties of Fe_2BiTaO_7 were characterized by XRD, SEM, TEM and UV-Vis diffuse reflectance spectroscopy. The results show that Fe_2BiTaO_7 crystallizes with the pyrochlore-type structure, cubic crystal system and space group *Fd*3*m*. The estimated band gap of Fe_2BiTaO_7 is 1.72 eV. The photocatalytic degradation of rhodamine B over Fe_2BiTaO_7, P25 TiO_2, N-doped TiO_2 and Bi_2InTaO_7 was investigated under visible light irradiation. The photocatalytic efficiency with Fe_2BiTaO_7 catalyst is 1.5 times of N-doped TiO_2 catalyst after 140 minutes under visible light irradiation. Fe_2BiTaO_7 has higher visible-light photocatalytic performance and shows much better activity than that of other photocatalysts. The photocatalytic degradation of rhodamine B follows the first-order reaction kinetics, and the first-order rate constant is 0.022 93 min^{-1} for Fe_2BiTaO_7. The possible photocatalytic degradation pathway of rhodamine B under visible light irradiation is suggested. In addition, the photocatalytic degradation of phenol over Fe_2BiTaO_7 catalyst was investigated under visible light irradiation. Fe_2BiTaO_7 (visible light) photocatalysis system is confirmed to be suitable for textile industry wastewater treatment.

Key words: catalysis; Fe_2BiTaO_7; optical properties; visible light; photocatalytic degradation; rhodamine B

收稿日期:2014-09-17。收修改稿日期:2014-11-13。

国家自然科学基金(No.21277067);中以科学与战略研究开发专项资金(No.5)资助项目。

*通讯联系人。E-mail:jfluan@nju.edu.cn

0 Introduction

Dyes in the effluents of the textile, leather, food processing, dyeing, paper, and manufacturing industries have become one of the most notorious organic pollutants in aquatic environments in recent years[1-6]. There is huge volume of dye wastewater releasing to the ecosystem each year, which causes serious environmental pollutions[7]. The presence of dye in water is not only aesthetically displeasing but also adverse to water transparency, resulting in reduction of sunlight penetration, gas solubility and reducing the photosynthetic reaction[3-4,8]. Some dyes also exhibit toxic effects toward microbial populations and some are even carcinogenic to mankind[9-10]. Rhodamine B(RhB) is one of the most important representatives of xanthene dyes widely utilized as a photosensitizer, a quantum counter and an active medium in dye lasers, etc. Most dyes are resistant to biodegradation and direct photolysis. As a N-containing dye, RhB undergoes natural reductive anaerobic degradation to yield potentially carcinogenic aromatic amines[11-12]. Therefore, the removal of RhB from wastewater is necessary and should be highly concerned.

Conventional methods including physical, chemical and biological processes are used for the removal of dyes[13-16]. However, it is usually inefficient to use biological oxidation or multi-step physical-chemical treatments for removing dye colors[17]. Photocatalysis has emerged as an efficient approach for purifying water[18-20]. In recent years, photosensitive degradation of colored contaminants in wastewater on semiconductor surface has attracted a great deal of attentions[21-25]. Zhao et al.[26] reported that some dyes could be degraded under visible light irradiation over TiO_2 by a self-photosensitized process. Some dyes are often utilized as a probe contaminant to evaluate the activity of a photocatalyst under irradiation of both ultraviolet light and visible light[27-28]. As the most commonly used photocatalyst, TiO_2 has shown effective photocatalytic activity for RhB under ultraviolet light irradiation accounted for 4% of sunlight. However, TiO_2 cannot be used in the visible light region which accounts for 43% of sunlight, and this problem limits its applications in the field of photocatalysis. Therefore, some efficient catalysts, which can generate electron-hole pairs under visible light irradiation, should be developed. Fortunately, there are some oxides such as $BiVO_4$, $Bi_{12}TiO_{20}$, $K_6Nb_{10.8}O_{30}$, $Bi_{38}ZnO_{58}$ which show photocatalytic activity under visible light irradiation[29-37]. Because of the controllability in composition, the diversity in structure and the difference in property, transition metal oxides nano-composite has been further developed in the field of photocatalysis. A series of $A_2B_2O_7$ inorganic compounds with different structures have been resulted from the wide-range chemical replacement in A, B and O site. In particular, $A_2B_2O_7$ compounds are considered to own better photocatalytic property under visible light irradiation[38-42], they have not only been the important part of the nano-materials field but also have a good application in real life. In our previous work[43], we found that Bi_2InTaO_7 crystallized with the pyrochlore-type structure which could be used as a photocatalyst under visible light irradiation. It seems that Bi_2InTaO_7 has a potential for improvement of photocatalytic activity by modification of its structure. According to above analysis, we guess that the substitution of Bi^{3+} by Fe^{5+} and substitution of In^{3+} by Bi^{3+} in Bi_2InTaO_7 may increase carriers concentration. A change and improvement of the electrical transportation and photophysical properties can be found in the Fe_2BiTaO_7 compound.

To the best of our knowledge, there have no reports on preparation and structural, photophysical and photocatalytic property characterizations for Fe_2BiTaO_7. The molecular composition of Fe_2BiTaO_7 is very similar to other $A_2B_2O_7$ compounds. The resemblance suggests that Fe_2BiTaO_7 may possess photocatalytic property under visible light irradiation, similar to that of other members in $A_2B_2O_7$ family. Fe_2BiTaO_7 also seems to have potential for improving the photocatalytic activity by modification of its structure.

We report here the synthesized semiconductor compound Fe_2BiTaO_7 and its photocatalytic property for photosensitized removal of colored contaminants in

wastewater under visible light irradiation. The structural, photophysical and photocatalytic property of Fe_2BiTaO_7 were investigated. A comparison among the photocatalytic property of Fe_2BiTaO_7, P25 TiO_2, N-doped TiO_2 and Bi_2InTaO_7 was performed in order to reveal the structure-photocatalytic activity relationship for the title compound.

1 Experimental

1.1 Preparation of Fe_2BiTaO_7 powder photocatalyst

The photocatalysts were synthesized by a solid-state reaction method[36]. Fe_2O_3, In_2O_3, Bi_2O_3 and Ta_2O_5 with purity of 99.99% (Sinopharm Group Chemical Reagent Co., Ltd., Shanghai, China) were utilized as precursors. All powders were dried at 200 ℃ for 4 h before synthesis. The precursors were stoichiometrically mixed prior to the synthesis of Fe_2BiTaO_7 and the mixture was then pressed into small columns and put into an alumina crucible (Shenyang Crucible Co., Ltd., China). Finally, calcination was carried out at 1 060 ℃ for 30 h in an electric furnace (KSL 1700X, Hefei Kejing Materials Technology CO., Ltd., China). Similarly, Bi_2InTaO_7 was prepared by calcination at 1 050 ℃ for 46 h.

1.2 Preparation of nitrogen-doped titania photocatalyst

Nitrogen-doped titania (N-doped TiO_2) catalyst with tetrabutyl titanate as a titanium precursor was prepared by using the sol-gel method at room temperature. 17 mL tetrabutyl titanate and 40 mL absolute ethyl alcohol were mixed as solution a, which was then added dropwise under vigorous stirring into a mixture (solution b) of 40 mL absolute ethyl alcohol, 10 mL glacial acetic acid and 5 mL double distilled water to form transparent colloidal suspension c. Subsequently aqua ammonia with n_N/n_{Ti} of 8% was added into c under vigorous stirring and stirred for 1 h. Finally, the xerogel was formed after being aged for 2 d. The xerogel was ground into powder and was then calcined at 500 ℃ for 2 h, subsequently was ground in agate mortar and screened by shaker to obtain N-doped TiO_2 powder.

1.3 Characterization of photocatalysts

The crystal structures of the photocatalysts were analyzed by the powder X-ray diffraction method (D/MAX-rB, Rigaku Corporation, Japan) with Cu $K\alpha$ radiation (λ=1.54 18 nm). The data were collected at 295 K with a step-scan procedure in the range of 2θ= 10°~95°. The step interval was 0.02° and the time per step was 1.2 s. The chemical composition of Fe_2BiTaO_7 was estimated by scanning electron microscope energy dispersive X-ray spectroscopy (SEM-EDS, LEO 1530VP, LEO Corporation, Germany). The contents of surface O^{2-}, Fe^{3+}, Bi^{3+} and Ta^{5+} in Fe_2BiTaO_7 were determined by X-ray photoelectron spectroscopy (XPS, ESCALABMK-2, VG Scientific Ltd., U.K.). The chemical composition within the depth profile of Fe_2BiTaO_7 was examined by the argon ion denudation method when X-ray photoelectron spectroscopy was utilized. The optical absorption of Fe_2BiTaO_7 was analyzed with an UV-Visible spectrophotometer (Lambda 40, Perkin-Elmer Corporation, USA). The surface area of Fe_2BiTaO_7 was determined by BET model (MS-21, Quantachrome Instruments Corporation, USA) with N_2 adsorption at liquid nitrogen temperature. The particle sizes of the photocatalysts were measured by malvern′s mastersize-2000 particle size analyzer (Malvern Instruments Ltd., United Kingdom). The particle morphology was measured by transmission electron microscope (Tecnal F20 S-Twin, FEI Corporation, USA).

1.4 Photocatalytic reaction

The photocatalytic degradation of RhB (Tianjin Kermel Chemical Reagent Co., Ltd.) was performed with 0.8 g photocatalyst (Fe_2BiTaO_7, P25 TiO_2, N-doped TiO_2 or Bi_2InTaO_7) powder suspended in 300 mL of 0.029 3 mmol·L^{-1} RhB solution within a pyrex glass cell (Jiangsu Yancheng Huaou Industry, China). Before visible light irradiation, the suspension was magnetically stirred in the dark for 45 min to ensure establishment of an adsorption/desorption equilibrium among the photocatalysts, RhB dye and atmospheric oxygen. The photocatalytic reaction system is consisted of a 300 W Xe arc lamp with the main emission wavelength at 436 nm (Nanjing JYZCPST

CO., Ltd.), a magnetic stirrer and a cut-off filter (λ> 400 nm, Jiangsu Nantong JSOL Corporation, China). The Xe arc lamp was surrounded by a quartz jacket and was positioned within the inner part of a photoreactor quartz vessel (5.8 cm in diameter and 68 cm in length), through which a suspension of RhB and photocatalyst was circulated. An outer recycling water glass jacket maintained a near constant reaction temperature (22 ℃), and the solution was continuously stirred and aerated. 2 mL aliquots were sampled at various time intervals. The incident photon flux I_o measured by a radiometer (Model FZ-A, Photoelectric Instrument Factory Beijing Normal University, China) was 4.76×10^{-6} Einstein·L^{-1}·s^{-1} under visible light irradiation (wavelength range of 400~700 nm). The incident photon flux on the photoreactor was varied by adjusting the distance between the photoreactor and the Xe arc lamp. The adjustment of pH value was not carried out and the initial pH value was 7.0. The concentration of RhB was determined according to the absorption at 554 nm by an UV-Vis spectrophotometer (Lambda 40, Perkin-Elmer Corporation, USA). The inorganic products obtained from RhB degradation were analyzed by ion chromatograph (DX-300, Dionex Corporation, USA).

The identification of RhB and the degradation intermediate products of RhB were performed by gas chromatograph-mass spectrometer (HP 6890 Series Gas Chromatograph, HP-Innowax column, 30 m×0.32 mm×0.25 μm) operated at 320 ℃ and connected to HP 5973 mass selective detector and a flame ionization detector with He as the carrier gas. The split ratio was 40:1, the injection and detector temperature were 250 ℃ and 300 ℃ respectively. Intermediate products of RhB were also identified by liquid chromatograph-mass spectrometer (LC-MS, Thermo Quest LCQ Duo, USA, HPLC column : Beta Basic-C18 (150 mm×2.1 mm×5 μm), Finnigan, Thermo, USA). Here, 20 μL of post-photocatalysis solution was injected automatically into the LC-MS system. The eluent contained 60% methanol and 40% water, and the flow rate was 0.2 mL·min^{-1}. MS conditions included an electrospray ionization interface and a capillary temperature of 27 ℃ with a voltage of 19.00 V, a spray voltage of 5 000 V and a constant sheath gas flow rate. The spectrum was acquired in the negative ion scan mode, sweeping the *m/z* range from 50 to 600. Evolution of CO_2 was analyzed with an intersmat™ IGC120-MB gas chromatograph equipped with a porapack Q column (30 m×0.32 mm×20 μm), which was connected to a catharometer detector.

The total organic carbon (TOC) concentration was determined with a TOC analyzer (TOC-5000, Shimadzu Corporation, Japan). The photonic efficiency was calculated according to the following equation[44-45]:

$$\varphi=R/I_o$$

where φ is the photonic efficiency (%), and R is the rate of RhB degradation (mol·L^{-1}·s^{-1}), and I_o is the incident photon flux (Einstein·L^{-1}·s^{-1}).

The catalyst recycling experiment was taken to prove that the Fe_2BiTaO_7 catalyst was still active. The Fe_2BiTaO_7 catalyst was washed by anhydrous ethanol and distilled water for 6 times after recycling from the previous experiment, then it was dried in the 60 ℃ oven and put it into the photocatalytic reactor for the degradation of rhodamine B again, the catalyst was recycled for three times.

2 Results and discussion

2.1 Structure analysis

Fig.1 shows the TEM image of Fe_2BiTaO_7 nanoscale particles and regular shapes. The diameter of Fe_2BiTaO_7 particles is 400~600 nm, indicating a small mean particle size. Fig.2(a) and (b) present SEM image and EDS spectrum of Fe_2BiTaO_7, respectively. SEM-EDS spectrum taken from the prepared

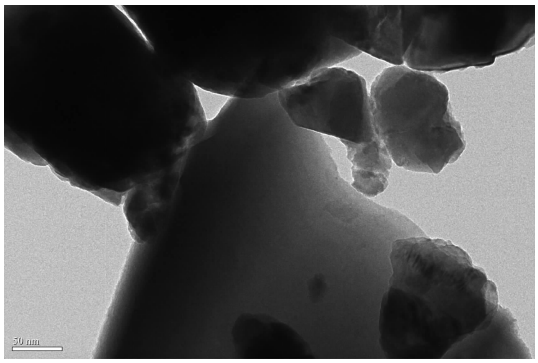

Fig.1 TEM image of Fe_2BiTaO_7

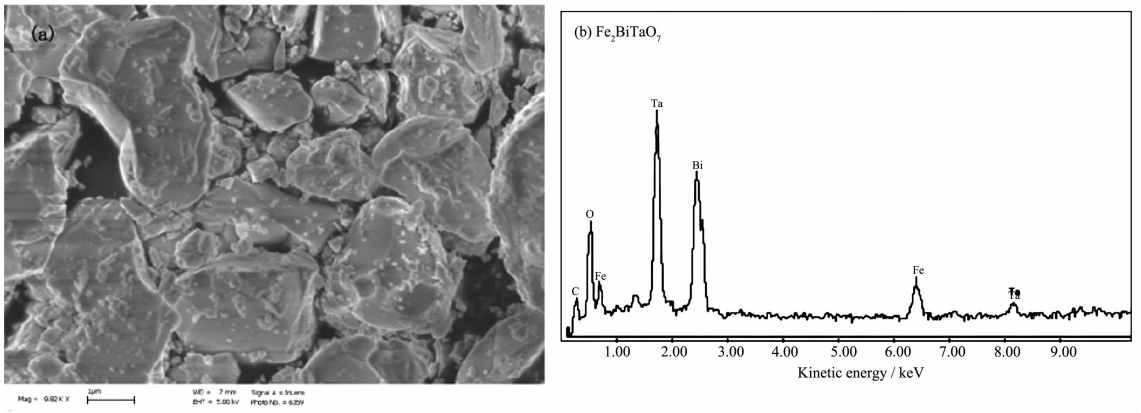

Fig.2　SEM image and EDS spectrum of Fe_2BiTaO_7

Fe_2BiTaO_7 indicates the presence of iron, bismuth, tantalum and oxygen. Other elements can not be identified from Fe_2BiTaO_7.

Fig.3 shows the XRD pattern of Fe_2BiTaO_7. The full-profile structure refinements of the collected data are obtained by the RIETAN™ [46] program based on Rietveld analysis. The results of the final refinements for Fe_2BiTaO_7 indicate a good agreement between the observed intensities and calculated intensities for the pyrochlore-type structure, a cubic crystal system and a space group *Fd*3*m* (O atoms are included in the model). The lattice parameter α for Fe_2BiTaO_7 is 1.048 734 4 nm. All the diffraction peaks for Fe_2BiTaO_7 can be indexed according to the lattice constant and the space group above. The atomic coordinates and structural parameters of Fe_2BiTaO_7 are listed in Table 1. It can be seen from Fig.3 that Fe_2BiTaO_7 is a single phase. In addition, the XRD results show that Fe_2BiTaO_7 crystallizes by the pyrochlore-type structure, a cubic crystal system and a space group *Fd*3*m*. The 2θ angles for each diffraction of Bi_2InTaO_7 change with Bi^{3+} substitution by Fe^{3+} and In^{3+} substitution by Bi^{3+}. The lattice parameter decreases from α=1.074 641 0 nm for Bi_2InTaO_7 to α=1.048 734 4 nm for Fe_2BiTaO_7, indicating a decrease in lattice parameter of the photocatalyst with a decrease of corresponding ionic radii, Fe^{3+} (0.078 nm)<Bi^{3+} (0.117 nm) and Fe^{3+} (0.078 nm)<In^{3+} (0.092 nm).

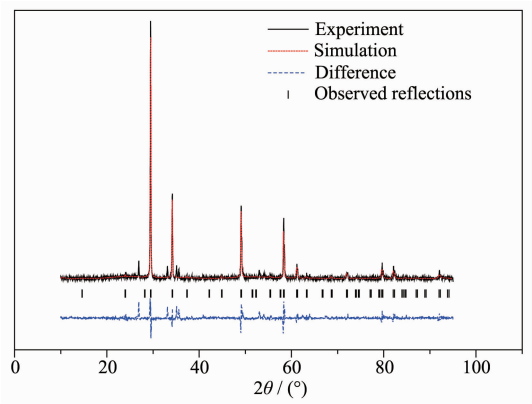

Fig.3　XRD patterns and Rietveld refinements for Fe_2BiTaO_7 prepared by a solid-state reaction method at 1 060 ℃

Fe_2BiTaO_7 and Bi_2InTaO_7 crystallize with the same pyrochlore-type structure according to the X-ray diffraction results. The cubic system structure with space group *Fd*3*m* for Bi_2InTaO_7 keep unchanged upon substituting Fe^{3+} by Bi^{3+} and substituting Bi^{3+} by In^{3+}. The outcome of refinements for Fe_2BiTaO_7 generates the unweighted R factors, R_P =18.64% with space

Table 1　Atomic coordinates and structural parameters of Fe_2BiTaO_7 prepared by the solid state reaction method

Atom	x	y	z	Occupation factor
Fe	0.000 00	0.000 00	0.000 00	1.0
Bi	0.500 00	0.500 00	0.500 00	0.5
Ta	0.500 00	0.500 00	0.500 00	0.5
O(1)	–0.100 00	0.125 00	0.125 00	1.0
O(2)	0.125 00	0.125 00	0.125 00	1.0

group *Fd*3*m*. The crystal structure of Bi_2InNbO_7 was refined by Zou et al.[47] and *R* factor obtained was large due to a slightly modified structure model for Bi_2InNbO_7. According to the high purity of the precursors utilized in this study and no impurity elements observed from EDS results, it is unlikely that the observed space groups originate from the impurities. Therefore, it is suggested that the slightly high R_P factor for Fe_2BiTaO_7 is due to a slightly modified structure model for Fe_2BiTaO_7. It should be emphasized that the defects or the disorder/order of a fraction of the atoms can result in the change of structures, including different bond-distance distributions, thermal displacement parameters and occupation factors for some of the atoms.

The various elemental XPS peaks and the corresponding specific binding energies of Fe_2BiTaO_7, i.e. Bi4$f_{7/2}$, Ta4$f_{7/2}$, Fe2$p_{3/2}$, O1*s*, are 155.9, 26.6, 708.2, 529.0 eV, respectively. The results further suggest that the oxidation states of Fe, Bi, Ta and O ions from Fe_2BiTaO_7 are +3, +3, +5 and −2 respectively. For Fe_2BiTaO_7, the average atomic ratios of Fe∶Bi∶Ta∶O are 2.00∶0.97∶1.01∶6.96 according to the average results of XPS, SEM-EDS. Similarly, the oxidation states of Bi, In, Ta and O ions from Bi_2InTaO_7 are +3, +3, +5 and −2 respectively. It is obvious that the observed XPS spectra of Fe_2BiTaO_7 show neither shoulders nor widening peaks, implying (albeit not proving) the absence of any other phases. Hence, it can be deduced that the obtained material is of high purity under our preparation conditions.

Fig.4 presents the selected area electron diffraction pattern of Fe_2BiTaO_7. It can be seen from Fig.4 that Fe_2BiTaO_7 is a single phase. As shown in Fig.4, Fe_2BiTaO_7 crystallizes with the pyrochlore-type structure, cubic crystal system and space group *Fd*3*m*. The lattice parameter for Fe_2BiTaO_7 is α=1.048 734 4 nm. According to the calculation results from Fig.4, the (*hkl*) value for the main peaks of Fe_2BiTaO_7 can be found and indexed.

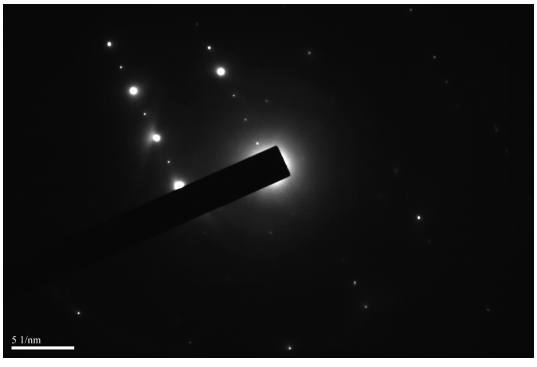

Fig.4 Selected area electron diffraction pattern of Fe_2BiTaO_7

2.2 UV-Vis diffuse reflectance spectroscopy

The absorption spectrum of Fe_2BiTaO_7 is presented in Fig.5. Compared with the well-known TiO_2 whose absorption edge is less than 380 nm, the absorption edge of newly synthesized Fe_2BiTaO_7 is at 710 nm, which is in the visible region of the spectrum. It is noteworthy that the apparent absorption (defined hereby as 1-transmission) can not take reflection and scattering into consideration. Consequently, the apparent absorbance at sub-bandgap wavelengths (600 to 800 nm for Fe_2BiTaO_7) is higher than zero.

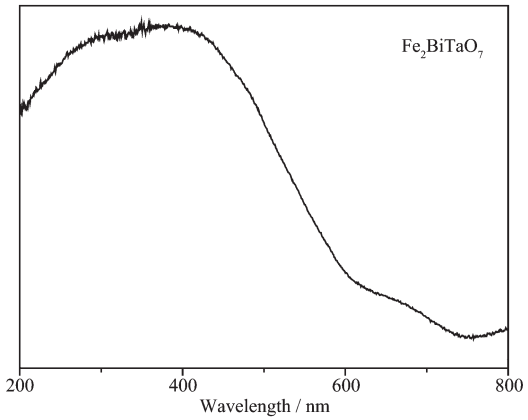

Fig.5 Absorption spectrum of Fe_2BiTaO_7

For a crystalline semiconductor, the optical absorption near the band edge follows the equation: $\alpha h\nu = A(h\nu - E_g)^n$ [48-49]. Here, A, α, E_g and ν are proportional constant, absorption coefficient, band gap and light frequency, respectively. Within the equation, n determines the character of the transition in a semiconductor. E_g and n can be calculated by the following steps: (i) plotting $\ln(\alpha h\nu)$ versus $\ln(h\nu - E_g)$ by assuming an approximate value of E_g, (ii) deducing the value of n according to the slope in the graph. (iii) refining the value of E_g by plotting $(\alpha h\nu)^{1/n}$ versus $h\nu$ and extrapolating the plot to $(\alpha h\nu)^{1/n}$=0. According to

this method, Fig.6 shows the plot of $(\alpha h\nu)^{1/n}$ versus $h\nu$ for Fe_2BiTaO_7. According to the data in Fig.6, the value of E_g for Fe_2BiTaO_7 is calculated to be 1.72 eV, while the value of n for Fe_2BiTaO_7 is 0.5. The results above indicate that Fe_2BiTaO_7 possesses a narrower band gap compared with Bi_2InTaO_7. At the same time, the optical transition for Fe_2BiTaO_7 is directly allowed.

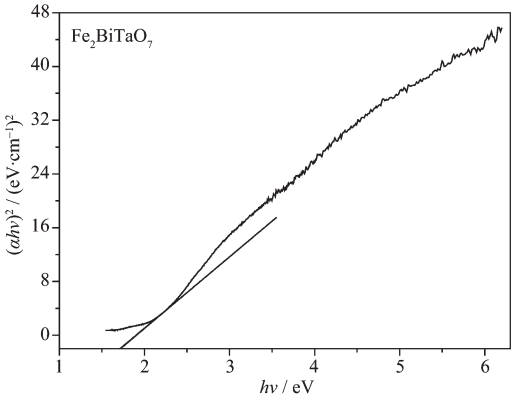

Fig.6　Plot of $(\alpha h\nu)^2$ versus $h\nu$ for Fe_2BiTaO_7

2.3 Photocatalytic activity

Generally speaking, the semiconductor photocatalysis starts from the direct absorption of supra-bandgap photons and the generation of electron-hole pairs in the semiconductor particles. Subsequently, the diffusion of the charge carriers to the surface of the semiconductor particles is followed. Fig.7 presents the concentration changes of RhB during the process of photocatalytic degradation under visible light irradiation (λ>400 nm) with the presence of Fe_2BiTaO_7, P25 TiO_2, N-doped TiO_2, Bi_2InTaO_7 as well as with the absence of photocatalyst. Above measurements are performed under oxygen-saturation conditions ($c_{O_2 sat}$ =1.02 mmol·L^{-1}). Though the photocatalyst/RhB suspension or RhB suspension exists in the experimental system, the degradation of RhB does not happen in dark. It can be clearly noticed from the results that a reduction of typical RhB peaks at 554 nm and 525 nm appear. Table 2 provides the photocatalytic effects with Fe_2BiTaO_7, P25 TiO_2, N-doped TiO_2 or Bi_2InTaO_7 as the catalyst under visible light irradiation (λ>400 nm). It can be seen from Table 2 that the photocatalytic efficiency is 95% with Fe_2BiTaO_7, 59% with P25 TiO_2, 63% with N-doped TiO_2, 37.5% with Bi_2InTaO_7 after 140 min under visible light irradiation. A complete color change from deep pink into colorless solution of the absorption signal is obtained with Fe_2BiTaO_7 within 230 min, which shows a complete degradation. According to the results, fast degradation rate is observed with Fe_2BiTaO_7 as the catalyst, and the photocatalytic degradation activity of Fe_2BiTaO_7 is higher than that of P25 TiO_2, N-doped TiO_2 or Bi_2InTaO_7. Furthermore, the photocatalytic degradation activity of N-doped TiO_2 is higher than that of P25 TiO_2 and Bi_2InTaO_7. Additionally, some decrease for the UV-Vis absorbance signal of RhB is obtained under visible light irradiation even in the absence of a photocatalyst. The initial rate of RhB degradation is

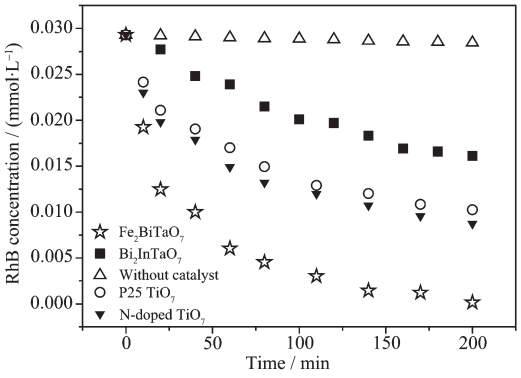

Fig.7　Photocatalytic degradation of rhodamine B under visible light irradiation with the presence of Fe_2BiTaO_7, P25 TiO_2, N-doped TiO_2, Bi_2InTaO_7 as well as with the absence of a photocatalyst

Table 2　Photocatalytic effects with Fe_2BiTaO_7, P25 TiO_2, N-doped TiO_2 or Bi_2InTaO_7 as the catalyst under visible light irradiation

Photocatalyst	Initial degradation rate /(nmol·L^{-1}·s^{-1})	Initial photonic efficiency/% (λ=420 nm)	Photocatalytic efficiency/% after 140 min under visible light irradiation
Fe_2BiTaO_7	2.430	0.051 05	95
P25 TiO_2	1.587	0.033 34	59
N-doped TiO_2	1.714	0.036 01	63
Bi_2InTaO_7	1.100	0.023 11	38

estimated to be 0.071 nmol·L^{-1}·s^{-1} and the photonic efficiency is 0.00149% (λ=420 nm) after visible light irradiation for 200 min with the absence of a photocatalyst. It suggests that the observed disappearance of RhB in the absence of a photocatalyst is due to direct dye-sensitization, and the dye-sensitization mechanism is similar to the observation from Liu et al.[50].

The degradation rate is almost 100% after visible light irradiation for 200 min with Fe_2BiTaO_7 as the catalyst, the catalyst is not in deactivation at this time. According to the experimental data, the degradation rate of the recycling experiment is 96%, 92%, 90%, respectively. Although the degradation rate drops each time, the change is not great, thus the results above can prove that the Fe_2BiTaO_7 catalyst is still active after the previous experiment, the property of Fe_2BiTaO_7 catalyst is stable and it can be recycled for photocatalysis many times.

The first order nature of the photocatalytic degradation kinetics with Fe_2BiTaO_7, P25 TiO_2, N-doped TiO_2 and Bi_2InTaO_7 as catalysts is clearly demonstrated in Fig.8, which presents a linear correlation between $\ln(C/C_0)$ (or $\ln(TOC/TOC_0)$) and the visible light irradiation time for the photocatalytic degradation of RhB with the presence of the photocatalysts. In above equation, C represents the RhB concentration at time t, and C_0 represents the initial RhB concentration, and TOC represents the total organic carbon concentration at time t and TOC_0 represents the initial total organic carbon concentration. According to the relationship between $\ln(C/C_0)$ and the irradiation time, the apparent first order rate constant k is 0.022 93 min^{-1} with Fe_2BiTaO_7, 0.006 27 min^{-1} with P25 TiO_2, 0.007 15 min^{-1} with N-doped TiO_2 and 0.003 29 min^{-1} with Bi_2InTaO_7, indicating that Fe_2BiTaO_7 is more efficient than P25 TiO_2, N-doped TiO_2 or Bi_2InTaO_7 for the photocatalytic degradation of RhB under visible light irradiation. In addition, N-doped TiO_2 is more efficient than P25 TiO_2 and Bi_2InTaO_7 for the photocatalytic degradation of RhB under visible light irradiation. According to the relationship between $\ln(TOC/TOC_0)$ and the irradiation time, the apparent first order rate constant k_{TOC} is estimated to be 0.019 22 min^{-1} with Fe_2BiTaO_7, 0.006 22 min^{-1} with P25 TiO_2, 0.006 73 min^{-1} with N-doped TiO_2 and 0.00317 min^{-1} with Bi_2InTaO_7, indicating that the photodegradation intermediate products of RhB probably appear during the photocatalytic degradation of RhB under visible light irradiation.

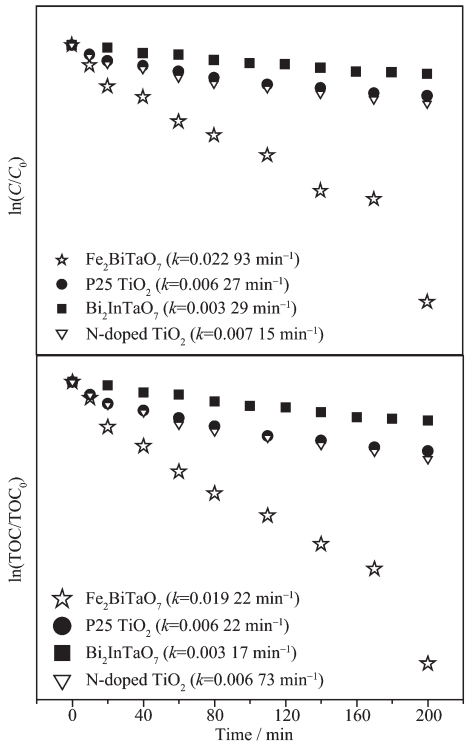

Fig.8 Observed first order kinetic plots for the photocatalytic degradation of rhodamine B with Fe_2BiTaO_7, P25 TiO_2, N-doped TiO_2 and Bi_2InTaO_7 as catalysts under visible light irradiation

In our experiments, the photodegradation intermediate products of RhB with Fe_2BiTaO_7 as the catalyst under visible light irradiation are identified as *N*,*N*-diethyl-*N*′-ethylrhodamine (*m*/*z*: 415.5), *N*,*N*-diethylrhodamine (*m*/*z*: 387.5), *N*-ethyl-*N*′-ethylrhodamine (*m*/*z*: 387.6), *N*-ethylrhodamine (m/z: 359.5) and rhodamine (*m*/*z*: 331.5), benzoic acid (m/z:122), terephthalic acid (*m*/*z*: 166), pentanedioic acid (*m*/*z*: 132), 3-Hydroxybenzoic acid (*m*/*z*: 138), 1,2-benzenedicarboxylic acid (*m*/*z*: 166) and maleic acid (*m*/*z*: 116), oxalic acid (*m*/*z*: 90), 2-hydroxypentanedioic acid (*m*/*z*: 148) and adipic acid (*m*/*z*: 146). Fig.9 suggests a possible photocatalytic degradation pathway

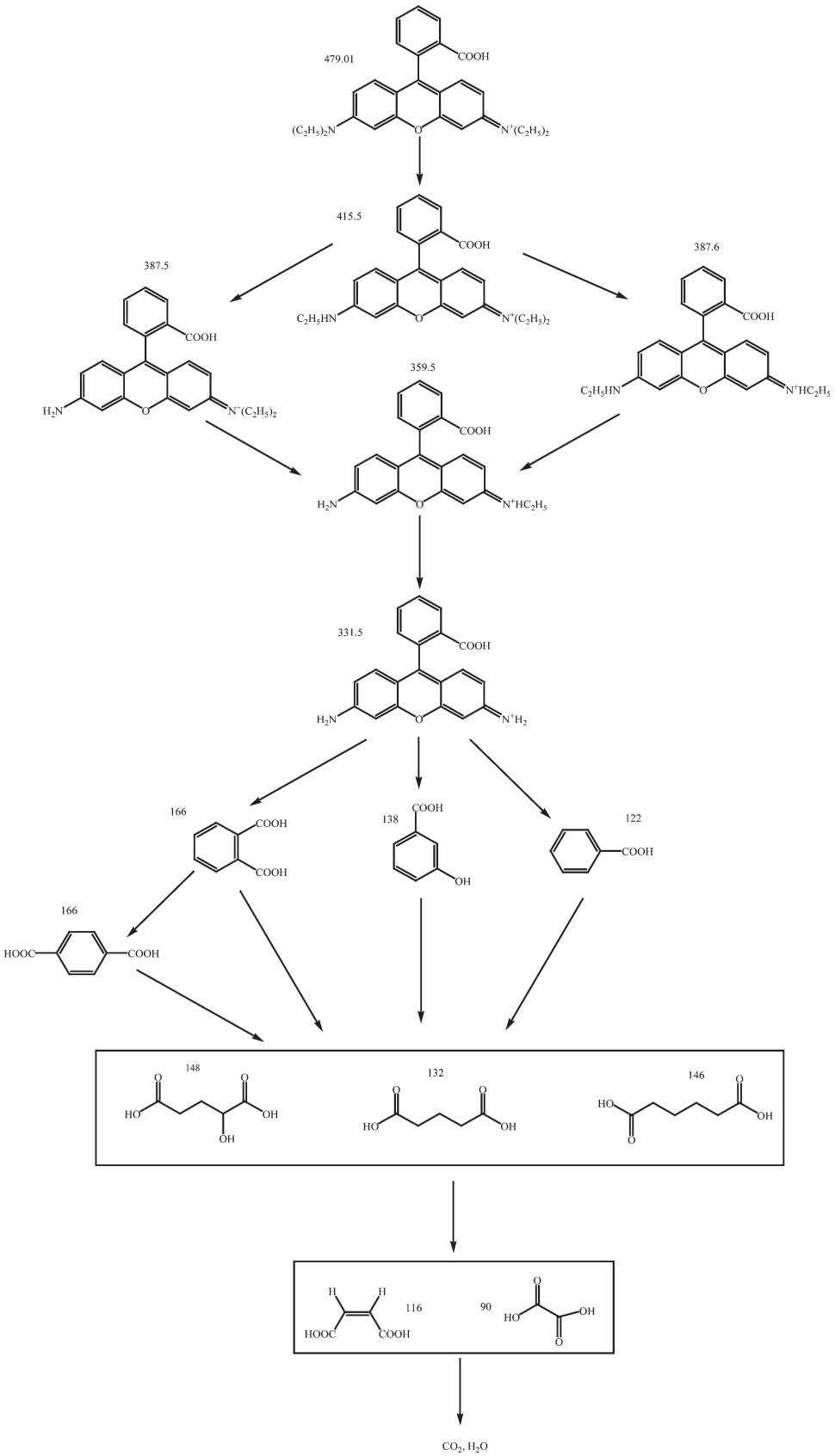

Fig.9　Suggested photocatalytic degradation pathway scheme for rhodamine B under visible light irradiation with the presence of Fe_2BiTaO_7

for RhB according to the intermediate products identified in this work. The main identified intermediates are the same as the results from Li et al.[51] for the TiO_2-assisted photodegradation of RhB under visible light irradiation. However, Zhong et al.[52] reported that the major intermediates of RhB during microwave-enhanced photocatalysis also include malonic acid, succinic acid, phthalic acid and 3-nitrobenzoic acid. In addition to benzoic acid, 2-hydroxypentanedioic acid, adipic acid, 3-hydroxybenzoic acid and terephthalic acid, He et al.[53] indentified the presence of succinic acid and phthalic acid as well in the process of photocatalytic degradation of RhB by Bi_2WO_6 with electron accepting agent under microwave irradiation.

The pathway was similar, but not identical to the pathway proposed by Horikoshi et al.[54] for the photodegradation of RhB under ultraviolet light irradiation and visible light irradiation assisted by microwave radiation with TiO_2 as the photocatalyst. According to the results of Li et al.[33], the RhB photodegradation occurs via two competitive processes: one process is N-demethylation, and the other process is the destruction of the conjugated structure. Thus, we consider that chromophore cleavage, ring-opening and mineralization should be the main photocatalytic degradation pathway of RhB in our work. RhB is converted to smaller organic species, and then mineralizes together with other organic groups to inorganic products such as CO_2 and water ultimately. Fig.10 presents the CO_2 yield during the photocatalytic degradation of RhB with Fe_2BiTaO_7, P25 TiO_2, N-doped TiO_2 or Bi_2InTaO_7 as the catalyst under visible light irradiation. The results show that the CO_2 yield increases gradually with increasing reaction time. The production rate of CO_2 with Fe_2BiTaO_7 is higher than that with P25 TiO_2, N-doped TiO_2 or Bi_2InTaO_7, which is in accordance with the absorption curve (Fig.5) of Fe_2BiTaO_7. The production amount of CO_2 is 0.241 03 mmol with Fe_2BiTaO_7 as the catalyst, 0.159 02 mmol with P25 TiO_2 , 0.166 73 mmol with N-doped TiO_2 and 0.108 03 mmol with Bi_2InTaO_7 in 300 mL reaction system after visible light irradiation for 200 min.

Fig.11 demonstrates the results of total organic

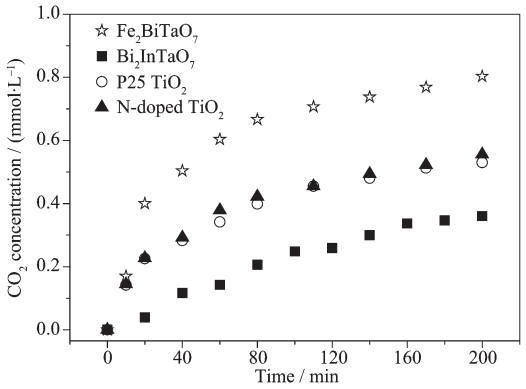

Fig.10 CO_2 production kinetics during the photocatalytic degradation of rhodamine B with Fe_2BiTaO_7, P25 TiO_2, N-doped TiO_2 and Bi_2InTaO_7 as catalysts under visible light irradiation

carbon (TOC) measurements. The results reveal that the total disappearance of organic carbon occurs after visible light irradiation for 230 min with Fe_2BiTaO_7 as the catalyst. The results show that after visible light irradiation for 140 min, 91% of TOC decrease is obtained with Fe_2BiTaO_7 as the photocatalyst, 59% with P25 TiO_2, 61% with N-doped TiO_2 and 37% with Bi_2InTaO_7. The turnover number (the ratio between the total amount of evolved gas and dissipative catalyst) is 0.185 for Fe_2BiTaO_7 after visible light irradiation for 200 min, suggesting that the reactions occur catalytically. The reactions stop when the light is turned off.

The photocatalytic property of the new compound Fe_2BiTaO_7 is notable under visible light irradiation.

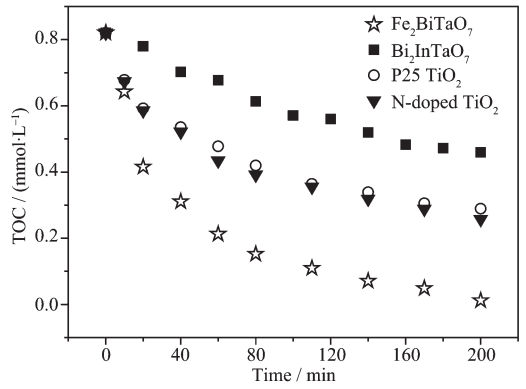

Fig.11 Disappearance of total organic carbon (TOC) during the photocatalytic degradation of rhodamine B with Fe_2BiTaO_7, P25 TiO_2, N-doped TiO_2 and Bi_2InTaO_7 as catalysts under visible light irradiation

This superior quality can be even more appreciated if we consider the fact that the specific surface area of Fe_2BiTaO_7 is apparently smaller than that of titanium dioxide. In our work, the BET specific surface area is 46 $m^2 \cdot g^{-1}$ for P25 TiO_2, 46 $m^2 \cdot g^{-1}$ for N-doped TiO_2, 2 $m^2 \cdot g^{-1}$ for Fe_2BiTaO_7 and 1 $m^2 \cdot g^{-1}$ for Bi_2InTaO_7 respectively. The specific surface area of Fe_2BiTaO_7 is almost 20 times smaller than that of P25 TiO_2.

The action spectra of RhB degradation with the presence of Fe_2BiTaO_7 under visible light irradiation show a clear photonic efficiency (0.03722% at its maximal point) at wavelengths corresponding to sub-Eg energies of Fe_2BiTaO_7 (λ from 710 to 800 nm). The existence of photonic efficiency at energies where photons are not absorbed by Fe_2BiTaO_7, in particular the correlation between the low-energy action spectrum and the absorption spectrum of RhB, demonstrates clearly that any photodegradation at wavelengths above 710 nm should be attributed to photosensitization by RhB itself (Scheme Ⅰ).

Scheme Ⅰ:

$$RhB_{(ads)} \xrightarrow{\text{Visible light}} RhB^*_{(ads)} \quad (1)$$

$$RhB^*_{(ads)} + Fe_2BiTaO_7 \rightarrow Fe_2BiTaO_7(e) + RhB^+_{(ads)} \quad (2)$$

$$Fe_2BiTaO_7(e) + O_2 \rightarrow Fe_2BiTaO_7 + \cdot O_2^- \quad (3)$$

According to the mechanism above, RhB adsorbed on Fe_2BiTaO_7 is excited by visible light irradiation. Subsequently an electron is injected from the excited RhB to the conduction band of Fe_2BiTaO_7 where the electron is scavenged by molecular oxygen. Scheme Ⅰ may explain the results obtained with Fe_2BiTaO_7 as the catalyst under visible light irradiation, where Fe_2BiTaO_7 may reduce recombination of photoinduced electrons and holes via the scavenging of electrons[56].

However, the situation for photocatalytic degradation mechanism of RhB is different below 710 nm, where the photonic efficiency correlates well with the absorption spectrum of Fe_2BiTaO_7. It evidently shows that the photocatalytic degradation mechanism of RhB is responsible for the photodegradation of RhB via band gap excitation of Fe_2BiTaO_7. Although detailed experiments about the effects of oxygen and water on the degradation mechanism of RhB are not performed, it is sensible to assume that the degradation mechanism of RhB in the first step is similar to the degradation mechanism of RhB observed for Fe_2BiTaO_7 under supra-bandgap irradiation, namely Scheme Ⅱ:

Scheme Ⅱ:

$$Fe_2BiTaO_7 \xrightarrow{\text{Visible light}} h^+ + e^- \quad (4)$$

$$e^- + O_2 \rightarrow \cdot O_2^- \quad (5)$$

$$h^+ + OH^- \rightarrow \cdot OH \quad (6)$$

The M-O-M bond angle is closer to 180°, and the excited state is more delocalized as shown by previous study[57], thus the charge carriers can move easily in the matrix. High diffusivity due to the mobility of the photoinduced electrons and holes helps impel more electrons and holes to reach the reactive sites on the catalyst surface, resulting in the improvement of the photonic efficiency of Fe_2BiTaO_7. The lattice parameter a=1.048 734 4 nm for Fe_2BiTaO_7 is smaller than the lattice parameter a=1.074 641 0 nm for Bi_2InTaO_7. Therefore, the photoinduced electrons and holes inside the particle of Fe_2BiTaO_7 are easier and faster to reach the reactive sites on the catalyst surface compared with those of Bi_2InTaO_7. As a result, the photocatalytic degradation activity of Fe_2BiTaO_7 is higher than that of Bi_2InTaO_7. The Bi-O-Ta bond angle of Fe_2BiTaO_7 is 121°, close to 180°. Thus, the photocatalytic activity of Fe_2BiTaO_7 is accordingly higher. In addition, the Bi-O-Ta bond angle of Fe_2BiTaO_7 is larger than the Bi-O-Ta bond angle of Bi_2InTaO_7, resulting in an increase of photocatalytic activity for Fe_2BiTaO_7 compared with Bi_2InTaO_7. The crystal structure of Fe_2BiTaO_7 is similar to that of Bi_2InTaO_7, but the crystal structures of Fe_2BiTaO_7 and P25 TiO_2 are different, and the electronic structures of them are also different. For Fe_2BiTaO_7, Fe is 3*d*-block metal element, and Bi is 6*p*-block metal element, and Ta is 5*d*-block metal element. But for Bi_2InTaO_7, Bi is 6*p*-block metal element, and In is 5*p*-block metal element, and Ta is 5*d*-block metal element. Moreover, for P25 TiO_2, Ti is 3*d*-block metal element, indicating that the photocatalytic activity may be affected by not only the crystal structure but also the electronic structure of the photocatalysts. The difference of the photocatalytic degradation activity of RhB among

Fe_2BiTaO_7, P25 TiO_2, N-doped TiO_2 and Bi_2InTaO_7 can be attributed mainly to the difference of their crystalline and electronic structures.

Fig.12 shows the suggested band structures of Fe_2BiTaO_7. Recently, the electronic structures of $InMO_4$ (M=V, Nb and Ta) and $BiVO_4$ have been reported by Oshikiri et al. according to the first principles calculations[58]. The conduction bands of $InMO_4$ (M=V, Nb and Ta) are mainly composed of a dominant orbital component from V3*d*, Nb4*d* and Ta5*d* orbitals, respectively. The valence bands of $BiVO_4$ are composed of a small Bi6*s* orbital component and a dominant O2*p* orbital component. The band structures of Fe_2BiTaO_7 should be similar to those of $InMO_4$ (M=V, Nb and Ta) and $BiVO_4$. Therefore, it can be concluded that the conduction band of Fe_2BiTaO_7 is composed of Ta5*d*, Fe3*d* and Bi6*p* orbitals, and the valence band of Fe_2BiTaO_7 is composed of a small dominant O2*p* orbital component and a small Bi6*s* orbital component. Direct absorption of photons by Fe_2BiTaO_7 can produce electron-hole pairs in the catalyst, showing that the necessary energy for decomposing RhB by photocatalysis should be larger than the band gap energy.

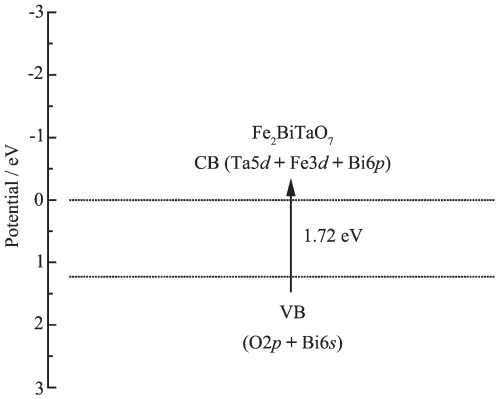

Fig.12 Suggested band structure of Fe_2BiTaO_7

In order to see the effect of light wavelength on the degradation efficiency of rhodamine B, rhodamine B is degraded with Fe_2BiTaO_7, P25 TiO_2, N-doped TiO_2 or Bi_2InTaO_7 as the catalyst under visible light irradiation (λ >500 nm). The results show that the photocatalytic efficiency is 42% with Fe_2BiTaO_7, 26% with P25 TiO_2, 28% with N-doped TiO_2, 17% with Bi_2InTaO_7 after 140 min under visible light irradiation.

RhB has a certain absorption in visible light area. In order to eliminate the influence of photosensitization, we have substituted phenol for RhB as the reaction substrate. The process of the experiment is as follows: The photocatalytic degradation of phenol is performed with 0.8 g photocatalyst (Fe_2BiTaO_7 or N-doped TiO_2) powder suspended in 300 mL of 0.029 3 mmol $\cdot L^{-1}$ phenol wastewater. The photocatalytic reaction system and initial experimental conditions are performed as the same as the previous experiment with RhB as the reaction substrate. The results show that the photocatalytic efficiency is 88% with Fe_2BiTaO_7, 62% with N-doped TiO_2 after 200 min under visible light irradiation. As phenol has no absorption effect in visible light area, the degradation of phenol can only be caused by photocatalysis. Thus, it can be deduced that Fe_2BiTaO_7 has a strong photocatalytic activity under visible light.

3 Conclusions

Fe_2BiTaO_7 was prepared by a solid-state reaction method. The structural, optical absorption and photocatalytic properties of Fe_2BiTaO_7 were investigated and compared with that of P25 TiO_2, N-doped TiO_2 and Bi_2InTaO_7. XRD results demonstrate that Fe_2BiTaO_7 crystallizes with the pyrochlore-type structure, cubic crystal system and space group *Fd*3*m*. The lattice parameter of Fe_2BiTaO_7 is found to be 1.048 734 4 nm. The band gap of Fe_2BiTaO_7 is estimated to be about 1.72 eV, indicating that Fe_2BiTaO_7 shows a strong optical absorption during the visible light region (λ > 400 nm). Photocatalytic degradation of aqueous RhB solutions is observed under visible light irradiation with the presence of Fe_2BiTaO_7 accompanied with the formation of end products such as carbon dioxide and water. Therefore, it can be concluded that Fe_2BiTaO_7/(Visible light) system may be regarded as an effective way for removing colored contaminants from waste water. Fe_2BiTaO_7 also shows higher photocatalytic activity for photocatalytic degradation of RhB under visible light irradiation compared with P25 TiO_2, N-doped TiO_2 and Bi_2InTaO_7. The photocatalytic degradation of RhB follows the first order reaction

kinetics. The apparent first order rate constant k is 0.022 93 min^{-1} with Fe_2BiTaO_7, 0.006 27 min^{-1} with P25 TiO_2, 0.007 15 min^{-1} with N-doped TiO_2 and 0.003 29 min^{-1} with Bi_2InTaO_7. The possible photocatalytic degradation pathway of RhB is provided in this paper. The results in our work prove that Fe_2BiTaO_7/(visible light) photocatalysis may be regarded as a method for practical treatment of diluted colored waste water. The Fe_2BiTaO_7/(visible light) photocatalysis system without demanding chemical reagents or using high pressure of oxygen or heating can be utilized for decolorization, purification and detoxification in textile industries, and printing and dyeing industries. In conclusion, the Fe_2BiTaO_7/(visible light) photocatalysis system may provide a valuable treatment for purifying and reusing colored aqueous effluents.

Acknowledgements: This work was supported by the National Natural Science Foundation of China (No.21277067), by a grant from China-Israel Joint Research Program in Water Technology and Renewable Energy (No.5). by a grant from the Natural Science Foundation of Jiangsu Province (No. BK20141312), by a project of science and Technology Development Plan of Suzhou City of China from 2014 (No. ZXG201440).

References:

[1] Annadurai G, Juang R S, Lee D J. *J. Hazard. Mater.*, **2002**, **92**(3):263-274

[2] Bhatnagar A, Jain A K. *J. Colloid Interface Sci.*, **2005**,**281** (1):49-55

[3] Su L, GanY X. *Composites Part B*, **2012**,**43**(2):170-182

[4] Wang S B, Boyjoo Y, Choueib A. *Chemosphere*, **2005**,**60** (10):1401-1407

[5] Shakir K, Elkafrawy A F, Ghoneimy H F, et al. *Water Res.*, **2010**,**44**(5):1449-1461

[6] Shen C S, Shen Y, Wen Y Z, et al. *Water Res.*, **2011**,**45**(16): 5200-5210

[7] Zhang F L, Zhao J C, Zang L, et al. *J. Mol. Catal. A*: *Chem.*, **1997**,**120**(1/2/3):173-178

[8] Brustein V P, Cavalcanti C L B, de Melo M R, et al. *Appl. Biochem. Biotechnol.*, **2012**,**166**(2):268-275

[9] Wang S B, Li H, Xu L Y. *J. Colloid Interface Sci.*, **2006**, **295**(1):71-78

[10]Guo Y P, Zhao J Z, Zhang H, et al. *Dyes Pigm.*, **2005**,**66** (2):123-128

[11]Fu H B, Pan C S, Yao W Q, et al. *J. Phys. Chem. B*, **2005**, **109**(47):22432-22439

[12]Ashraf U, Chat O A, Dar A A. *Chemosphere*, **2014**,**99**:199-206

[13]Parida K M, Sahu N, Biswal N R, et al. *J. Colloid Interface Sci.*, **2008**,**318**(2):231-237

[14]Mahmoodi N M, Najafi F. *Microporous Mesoporous Mater.*, **2012**,**156**:153-160

[15]Park H O, Oh S, Bade R, et al. *KSCE J. Civ. Eng.*, **2011**,**15** (3):453-461

[16]Chatha S A S, Asgher M, Ali S, et al. *Carbohydr. Polym.*, **2012**,**87**(2):1476-1481

[17]Xie Y B, Yuan C W, Li X Z. *Colloid Surf. A*, **2005**,**252** (1):87-94

[18]Pan H Q, Li X K, Zhuang Z J, et al. *J. Mol. Catal. A*: *Chem.*, **2011**,**345**(1/2):90-95

[19]Luan J F, Wang S, Ma K, et al. *J. Phys. Chem. C*, **2010**,**114** (20):9398-9407

[20]Rauf M A, Ashraf S S. *Chem. Eng. J.*, **2009**,**151**(1/2/3):10-18

[21]Chatterjee D, Mahata A. *J. Photochem. Photobiol. A-Chem.*, **2002**,**153**(1/2/3):199-204

[22]Kyung H, Lee J, Choi W Y. *Environ. Sci. Technol.*, **2005**,**39** (7):2376-2382

[23]Su L S, Gan Y X. *Composities Part B*, **2012**,**43**(2):170-182

[24]Dubal D P, Dhawale D S, More A M, et al. *J. Mater. Sci.*, **2011**,**46**(7):2288-2293

[25]Bao N, Li Y, Yu X H, et al. *Environ. Sci. Pollut. Res. Int.*, **2013**,**20**(2):897-906

[26]Qu P, Zhao J C, Shen T, et al. *J. Mol. Catal. A*: *Chem.*, **1998**,**129**(2-3):257-268

[27]Ghosh J P, Sui R H, Langford C H, et al. *Water Res.*, **2009**, **43**(18):4499-4506

[28]Adhikari R, Gyawali G, Sekino T, et al. *J. Solid State Chem.*, **2013**,**197**:560-565

[29]Zhang X, Ai Z H, Jia F L, et al. *Mater. Chem. Phys.*, **2007**, **103**(1):162-167

[30]Zhou J K, Zou Z G, Ray A K, et al. *Ind. Eng. Chem. Res.*, **2007**,**46**(3):745-749

[31]Zhang G K, Zou X, Gong J, et al. *J. Alloys Compd.*, **2006**, **425**(1/2):76-80

[32]Feng P, Chen C L, Hao Y, et al. *Mater. Chem. Phys.*, **2009**, **116**(1):294-299

[33]Li J P, Zhang X, Ai Z H, et al. *J. Phys. Chem. C*, **2007**,**111** (18):6832-6836

[34]Li X K, Kako T, Ye J H. *Appl. Catal. A*: *Gen.*, **2007**,**326**(1): 1-7

[35]Hou L R, Yuan C Z, Peng Y. *J. Mol. Catal. A*: *Chem.*, **2006**, **252**(1/2):132-135

[36]Tang X D, Ye H Q, Liu H, et al. *Chem. Phys. Lett.*, **2009**, **484**(1/2/3):48-53

[37]Dong H J, Chen G, Sun J X, et al. *Appl. Catal. B*: *Environ.*, **2013**,**134**:46-54

[38]Li K W, Wang H, Yan H. *J. Mol. Catal. A*: *Chem.*, **2006**,**249** (1/2):65-70

[39]Luan J F, Pan B C, Paz Y, et al. *Phys. Chem. Chem. Phys.*, **2009**,**11**(29):6289-6298

[40]Luan J F, Li M, Ma K, et al. *Chem. Eng. J.*, **2011**,**167**(1): 162-171

[41]Yang H, Li J, Wang L Y, et al. *Catal. Commun.*, **2013**,**35**: 101-104

[42]Nashim A, Parida K M. *Chem. Eng. J.*, **2013**,**215**:608-615

[43]Luan J F, Zhao W, Feng J W, et al. *J. Hazard. Mater.*, **2009**, **164**(2/3):781-789

[44]Marugan J, Hufschmidt D, Sagawe G, et al. *Water Res.*, **2006**,**40**(4):833-839

[45]Sakthivel S, Shankar M V, Palanichamy M, et al. *Water Res.*, **2004**,**38**(13):3001-3008

[46]Fazey P G, Oconnor B H, Hammond L C. *Clays Clay Miner.*, **1991**,**39**(3):248-253

[47]Zou Z, Ye J, Arakawa H. *J. Mater. Sci. Lett.*, **2000**,**19**(21): 1909-1911

[48]Tauc J, Grigorov R, Vancu A. *Phys. Status Solidi*, **1966**,**15** (2):627-637

[49]Butler M A. *J. Appl. Phys.*, **1977**,**48**(5):1914-1920

[50]Liu G M, Wu T X, Zhao J C, et al. *Environ. Sci. Technol.*, **1999**,**33**(12):2081-2087

[51]Li J Y, Ma W H, Lei P X, et al. *J. Environ. Sci.*, **2007**,**19** (7):892-896

[52]He Z, Yang S G, Ju Y M, et al. *J. Environ. Sci.*, **2009**,**21**(2): 268-272

[53]He Z, Sun C, Yang S G, et al. *J. Hazard. Mater.*, **2009**,**162** (2/3):1477-1486

[54]Oshikiri M, Boero M, Ye J H, et al. *J. Chem. Phys.*, **2002**, **117**(15):7313-7318